Host Pigment Epithelium-Derived Factor (PEDF) Prevents Progression of Uveal Melanoma Metastasis in the Liver

John M. Lattier, BS[1], **Hua Yang, MD, PhD**[1], **Susan Crawford, DO**[2], and **Hans E. Grossniklaus, MD, MBA**[1]

[1]Department of Ophthalmology, Emory University, Atlanta, GA

[2]Department of Pathology, University of St. Louis, St. Louis, MO

Abstract

Uveal melanoma (UM) has a 30% five-year mortality rate, primarily due to liver metastasis. Both angiogenesis and stromagenesis are important mechanisms for the progression of liver metastasis. Pigment epithelium-derived factor (PEDF), an anti-angiogenic and anti-stromagenic protein, is produced by hepatocytes. Exogenous PEDF suppresses metastasis progression; however, the effects of host-produced PEDF on metastasis progression are unknown. We hypothesize that host PEDF inhibits liver metastasis progression through a mechanism involving angiogenesis and stromagenesis. Mouse melanoma cells were injected into the posterior ocular compartment of PEDF-null mice and control mice. After one month, the number, size, and mean vascular density (MVD) of liver metastases were determined. The stromal component of hepatic stellate cells (HSCs) and the type III collagen they produce was evaluated by immunohistochemistry. Host PEDF inhibited the total area of liver metastasis and the frequency of macrometastases (diameter >200μm) but did not affect the total number of metastases. Mice expressing PEDF exhibited significantly lower MVD and less type III collagen production in metastases. An increase in activated HSCs was seen in the absence of PEDF, but this result was not statistically significant. In conclusion, host PEDF inhibits the progression of hepatic metastases in a mouse model of UM, and loss of PEDF is accompanied by an increase in tumor blood vessel density and type III collagen.

Keywords

PEDF; uveal melanoma; metastasis; angiogenesis; stromagenesis

INTRODUCTION

Uveal melanoma (UM) originates in melanocytes in the choroid, ciliary body, or iris, collectively known as the uvea. In the United States, UM is the most common form of eye cancer in adults with 5.1 cases per million [1]. Caucasians account for 98% of cases, with fair skin and light-colored eyes among the risk factors [2,1]. Data regarding ultraviolet light exposure as a risk factor for UM have been inconclusive [3-5]. Familial UM is rare, accounting for only 0.6% of cases [6]. Treatment of UM has recently shifted away from enucleation (removal of the eye) towards irradiation and plaque radiotherapy, but the 5-year survival rate has remained unchanged at 80% over the last 40 years [7,1]. This is because the

Correspondence to Dr. Hans E. Grossniklaus, BT428, Emory Eye Center, Atlanta, GA 30307, Tel 404-778-4616, Fax 404-778-4610, ophtheg@emory.edu.

CONFLICT OF INTEREST
The authors declare that they have no conflict of interest.

cause of death in patients with metastatic UM is most commonly due to hepatic metastasis and liver failure, suggesting that metastasis occurs before treatment of the primary tumor [7]. In humans, when UM metastasizes to the liver, it initially appears to form dormant, avascular metastases that are too small to be imaged [8,9]. Gene expression profiling or multiplex ligation probe amplification can be used to predict which UM patients will develop aggressive metastases [10-12].

The liver is the main site of metastasis in 80% of patients with UM who develop metastatic disease [7]. One hypothesis as to why UM cells predominantly metastasize to the liver is that passive, mechanical factors such as the location of the liver in the vascular path and the trapping of cells in the liver vasculature cause cancer cells to deposit in the liver [13]. Another hypothesis is that UM surface receptors CXCR4 and c-Met mediate migration toward ligand gradients produced by the liver, namely stromal cell-derived factor (SDF) and hepatocyte growth factor (HGF) [14]. Micrometastases (around 4 to 16 cells, diameter $<50\mu m$) may stay quiescent for years [9,15]. At some point, these micrometastatic colonies may enlarge to form intermediate metastases (diameter 50-500μm in humans, 50-200μm in mice) or larger still to form macrometastases (diameter $>500\mu m$ in humans, $>200\mu m$ in mice) [9]. What triggers activation from dormancy is unknown; however, there are several properties of the UM cell and of the host liver microenvironment that may potentiate metastatic progression.

Intrinsic properties of the UM cell, such as monosomy 3, correlate strongly with highly metastatic UM and mortality [16,17]. Mutations in the deubiquitinating enzyme BRCA1-associated protein (BAP1) located on chromosome 3 are seen almost exclusively in patients with metastatic UM [18]. In addition, tumor cells upregulate factors that may enhance metastatic progression such as fibronectin 1, insulin receptor substrate 2 (IRS2), and matrix metalloproteinase 2 (MMP2) [19]. Metastatic UM cells may also downregulate HLA antigen expression and evade the host immune response [20].

Extrinsic, or host, properties may also play an important role in suppressing or promoting metastatic tumor progression. Angiogenesis, or the formation of new blood vessels to supply the tumor with nutrients and oxygen, is necessary for metastases to grow larger than 2-3mm^3 [21]. As the metastases grow, tumor cells become hypoxic and release vascular endothelial growth factor (VEGF) into the tumor microenvironment, recruiting host vascular endothelial cells. Additionally, stromagenesis is an important and often overlooked component of metastatic progression [22]. Stromagenesis in the liver includes the activation of hepatic stellate cells (HSCs) into a migratory and proliferative state, in addition to the formation of extracellular matrix components such as type I and III collagen and the secretion of growth factors [23,13]. The extracellular matrix provides a scaffold for blood vessel and tumor cell growth, meanwhile growth factors such as VEGF promote angiogenesis and metastatic progression [13].

A candidate host-produced factor, and one of the most potent inhibitors of angiogenesis and stromagenesis, is pigment epithelium-derived factor (PEDF). PEDF is a secreted protein that is produced by hepatocytes but downregulated in hypoxic cutaneous melanoma cells [24-27]. PEDF binds the receptors PNPLA2, laminin receptor, and ATP synthase [28-30]. PEDF induces apoptosis of the endothelial cell, inhibiting angiogenesis, and this occurs through multiple pathways including Fas/FasL and cleavage of caspases 8 and 9 [31,32]. In addition, PEDF inhibits VEGF receptors 1 and 2 [33,34]. PEDF inhibits stromagenesis by causing apoptosis in HSCs and by causing the cytoskeleton of surviving HSCs to break down [26]. Deficiency in PEDF leads to increased pancreatic cancer invasiveness, hyperplasia, and disease morphology in mice, while human patients with pancreatic cancer have decreased levels of PEDF in serum and tumor cells [35]. PEDF is inhibited in hypoxic

environments and degraded by matrix metalloproteinases MMP-2 and MMP-9 which are secreted by tumor cells and macrophages, suggesting that as metastases progress, they downregulate host PEDF [36,25,37]. The VEGF/PEDF ratio has been suggested as an angiogenic switch in UM metastasis [38,39]. B16-LS9 melanoma cells that were transfected to overexpress PEDF and were injected into the eye of C57BL/6 mice exhibit decreased growth of primary tumor and decreased number of metastases in the liver, suggesting an anti-proliferative role of PEDF in cancer cells [40]. However, there have been no studies to date that have analyzed the role of specifically host-produced PEDF in suppressing metastatic UM progression [41,40].

The aim of this study is to uncover the role of an anti-angiogenic and anti-stromagenic factor produced by the host liver, PEDF, with regards to the progression of hepatic metastasis of UM. We used an established mouse model of UM in a strain of transgenic PEDF-null mice to examine properties of liver metastasis in the presence versus absence of host-produced PEDF.

METHODS

All experiments were performed in conduct with the Association for Research in Vision and Ophthalmology (ARVO) Statement for the Use of Animals in Ophthalmic and Visual Research and with Institutional Animal Care and Use Committee (IACUC) policies and procedures.

Cell culture

B16-LS9 mouse melanoma cells were cultured at 37°C and 5% CO_2. Cells were fed every 2-3 days in RPMI-1640 with 10% FBS, L-glutamine, HEPES, 1% non-essential amino acids, 1% sodium pyruvate, 1% MEM vitamin solution, and 1% penicillin-streptomycin. Before use in animal experiments, cells were trypsinized and suspended at $1.5 \times 10^5/1.5\mu L$ in phosphate buffer solution. Separate cultures were lysed with radioimmunoprecipitation assay buffer for use in western blot (50μg protein blotted with AB-PEDF1 antibody by BioProducts of Maryland, 1/5000). Human PEDF protein was used as a positive control (BioProducts of Maryland, 4ng per lane), with an expected band 50-75 kDa, and actin was used as a loading control (Millipore MAB1501, 1/5000). B16-LS9 melanoma cells are a representative model of human melanoma due to their high levels of c-Met expression and their propensity to metastasize to the liver [42,43].

Mouse model of uveal melanoma

PEDF-null mice were previously generated on a C57BL/6 background [44]. These mice are viable and have no known development deficiencies aside from being slightly overweight and exhibiting fatty liver [45]. Genotyping was confirmed by tail snip PCR analysis. Liver PEDF mRNA levels were determined by quantitative real-time polymerase chain reaction (n=4) of liver lysate collected in TRIzol reagent (Invitrogen Corp.). PEDF forward primer sequence was AAGGTCCCTGTGAACAAGC, and reverse primer sequence was GTCGTAGTAGAGAGCCCGGT. Protein expression was determined by immunohistochemistry of liver sections (n=3, antibody sc-16596 by Santa Cruz Biotechnology, Inc., 1/50) or western blot of 200μg liver lysates (n=3, antibody AB-PEDF1 by BioProducts of Maryland, 1/5000). Human PEDF protein was used as a positive control (BioProducts of Maryland, 4ng per lane), with an expected band 50-75 kDa, and actin was used as a loading control (Millipore MAB1501, 1/5000). Wild-type C57BL/6 mice were obtained from Charles River Labs; 7-week old female mice were anesthetized by intraperitoneal injection of 100mg/kg ketamine and 12mg/kg xylazine mixture in phosphate buffer solution. B16-LS9 cells were injected into the uveal layer of the right eye by first

preparing a passageway using a 30 gauge needle then by injecting $1.5 \times 10^5/1.5\mu L$ cells into the passageway [43]. Seven days post-injection, the right eye was enucleated, a method that precludes direct extraocular extension of the melanoma and promotes growth of liver metastases [43,46], and the eyes were stored in formalin. Twenty-eight days post-injection the mice were euthanized and livers were collected and routinely processed for histologic examination. Formalin fixed paraffin embedded slides of eyes and livers were prepared for use in staining procedures. A 7μm thick hematoxylin and eosin (H&E) stained section through the center of the eye containing the pupil, optic nerve, and maximum thickness of the melanoma was utilized for determining intraocular tumor size (n=4). Three 7μm thick H&E stained sections through the centers of the livers of each mouse (n=5) were used to determine metastatic melanoma size and frequency per previous protocols [47]. Unstained sections were used for histochemical and immunohistochemical staining. Eye and liver sections were obtained from the same set of mice.

Metastasis size and frequency assays

Formalin-fixed paraffin-embedded slides were stained with hematoxylin and eosin (H&E) and viewed using an Olympus DP-12 microscope (Tokyo, Japan). Three liver sections per mouse were measured, with five mice per genotype. The sizes of all metastases from a single liver section were summed to produce a total metastasis area value in μm^2 and this value was averaged across three sections per mouse. The total liver size was also measured, creating a ratio of metastasis size per liver size for normalization. Wild-type mouse metastasis area was set to 1.0 for comparison. Metastatic frequency was calculated by totaling the number of metastases of all sizes and normalizing by liver area. Additionally, the metastases were separated by size, where micrometastases have a diameter of less than $50\mu m^2$, intermediate metastases have a diameter of $50-200\mu m^2$, and macrometastases have a diameter greater than $200\mu m^2$, with sizes slightly different from the categorization in humans. These data were reported as a ratio per liver area, and all measurements were performed in triplicate sections that represented the liver as a whole (n=5).

Staining assays

Mean vascular density was determined through use of H&E staining or periodic acid-Schiff staining without hematoxylin. A cross section of a lumen lined with endothelial cells counted as one blood vessel, while tracts and branches were counted as separate vessels. The number of blood vessels per area was determined for both metastatic tissue and surrounding liver tissue (n=5) [48]. HSCs were visualized by smooth muscle actin (SMA) immunostaining (Mako M0851, 1:160) and analyzed by ImageJ (Version 1.45s, National Institutes of Health, Washington, DC) on a scale of 0:black to 255:white. In order to estimate tumor stromal component, reticulin staining was performed for type III collagen within the metastases (n=5). Fibers were manually traced and quantified by ImageJ.

Statistical analysis

Comparison of the three groups (PEDF+/+, PEDF+/-, and PEDF-/- mice) for all assays was performed using one-way analysis of variance (ANOVA) with the Newman-Keuls post-test to determine statistical significance among pairs. When comparing metastasis types among three groups, a two-way ANOVA with a Bonferroni post-test was utilized. We defined $p<0.05$ as denoting statistical significance for all assays and reported data with standard error of the mean. An unpaired t-test was used to analyze densitometry of the western blot.

RESULTS

Mouse model of uveal melanoma

To establish our mouse model of PEDF deficiency, we measured PEDF mRNA and protein levels in the livers of PEDF+/+ and PEDF-/- mice. PEDF+/+ mice express PEDF mRNA in the liver, whereas PEDF mRNA is absent from PEDF-/- mouse liver (Suppl. Fig. 1). Cycle threshold was reached after 21.7 cycles in PEDF+/+ mice and 33.7 cycles in PEDF-/- mice. Liver PEDF protein in PEDF+/+ and PEDF-/- mice was assayed by immunohistochemistry (Suppl. Fig. 2a) and western blot (Suppl. Figs. 2b,c). Both assays demonstrated an abundance of PEDF protein in the livers of PEDF+/+ mice but not in livers of PEDF-/- mice. B16-LS9 melanoma cells express PEDF in culture as expected (Suppl. Fig. 3). The eyes collected at day 7 showed that primary tumors were of equivalent size regardless of PEDF genotype (Fig. 1). Thus we conclude that this is an appropriate model with which to study the role of liver-produced PEDF on UM metastasis.

Metastasis size and frequency

PEDF+/- mice exhibited a 7.1 fold increase in metastasis area per liver section than PEDF+/+ mice, and PEDF-/- mice showed a 34.6 fold increase, both significantly greater than wild-type (Fig. 2). There was no statistical difference in the total number of metastases per liver section across the three genotypes (Fig. 3a). However, wild-type mouse livers contained predominantly micrometastases, PEDF+/- mice contained more intermediate metastases and several macrometastases, and PEDF-/- mice contained significantly more macrometastases than either wild-type or PEDF+/- mice (Fig. 3b). These data clearly demonstrate that the loss of host PEDF leads to a significant increase in the size of the metastatic tumor.

Angiogenesis: mean vascular density

PEDF+/- mice showed a 7.3 fold increase in mean vascular density (MVD), or blood vessels per 40x high-powered field of magnification (40HPF), versus PEDF+/+ controls, and the MVD of PEDF-/- mice was 20.8 fold greater than wild-type, both significantly greater ($p < 0.05$) (Fig. 4). Additionally, both PEDF-/- and PEDF+/- mice had significantly greater MVD in metastases than surrounding liver tissue, while WT mice did not. MVD of non-metastatic liver tissue was equivalent across the three genotypes. These findings corroborate a well-known function of PEDF, suggesting that PEDF may inhibit angiogenesis, or the formation of new blood vessels, in the metastases in mouse liver, but not vasculogenesis, or the formation of blood vessels during embryonic development. However, increased vascular density is a common result of metastatic progression, thus the relationship to loss of host PEDF may only be indirect.

Stromagenesis: hepatic stellate cell and type III collagen immunohistochemistry

A trend toward greater activated HSC density was found only in PEDF-/- mice but not PEDF+/- mice; however, this was not significantly different among the three groups (Fig. 5). There was however significantly less type III collagen, a marker for basement membrane production, in PEDF+/+ mice versus both PEDF+/- and PEDF-/- mice (Fig. 6). Type III collagen was not seen in micrometastases but was prevalent in both intermediate and macrometastases. These data suggest that HSCs are activated in micrometastases even in the presence of PEDF, and only slightly more so in the absence of PEDF, but that their production of extracellular matrix is delayed until at least the intermediate metastasis phase.

DISCUSSION

Stephen Paget proposed the "seed and soil" hypothesis in the late 1800s to explain why given forms of cancer are able to thrive in certain end organs [49]. He suggested that each

type of cancer, the seed, is only able to metastasize to organs that resemble its original microenvironment, the soil. By this reasoning, the end organ must be expressing factors that potentiate or suppress the growth of the metastasizing cancer cells. Indeed, key mediators of angiogenesis such as vascular endothelial growth factor (VEGF) and hypoxia-inducible factors (HIFs) are involved in end organ angiogenesis and growth of metastatic cancer [50-52]. Now we have shown that pigment epithelium-derived factor (PEDF) is also an important factor produced by the host that suppresses metastatic progression, and loss of PEDF is accompanied by an increase in angiogenesis and stromagenesis within the metastases.

PEDF produced and secreted by hepatocytes is thought to suppress metastasis in two ways. By interrupting the VEGF signaling cascade and inducing apoptosis in endothelial cells, PEDF suppresses the angiogenesis necessary for metastatic progression. By disrupting the cytoskeleton of HSCs and inducing their apoptosis, PEDF inhibits stromagenesis. In a hypothetical model, in healthy hepatic tissue the PEDF-VEGF ratio favors PEDF. VEGF is not being produced by tumor cells or HSCs, endothelial cell growth is not being recruited, and MMP-2 and MMP-9 are not being produced by melanoma cells or endothelial cells to degrade PEDF. However in the metastatic microenvironment, as the metastasis grows, it becomes hypoxic. VEGF and MMPs are produced, leading to the downregulation of PEDF and the unimpeded formation of stroma and growth of blood vessels. This process of breaking down the balance between PEDF and hypoxia appears to occur over several years. However, in PEDF-/- mice, the PEDF-VEGF balance is lost, stromagenesis and angiogenesis are potentiated, and this hypothetically leads to enlargement of the metastases over the span of one month.

Despite the production of PEDF by B16-LS9 cells in the tumor microenvironment, our data clearly demonstrate that metastatic progression is increased when hostproduced PEDF is knocked out. This effect is due to the increased presence of macrometastases of 200μm diameter or more. We have shown when host PEDF is lost the mean vascular density rises significantly, but only in metastatic tissue and not in liver tissue. This suggests that PEDF may play role in angiogenesis during metastasis but not vasculogenesis during development. Furthermore, we found that activated HSC density was slightly increased in PEDF-null mice, but this result was not statistically significant. This suggests that HSCs are activated at an early point in metastatic progression and only slightly responsive to PEDF *in vivo*. However, type III collagen normally produced by activated HSCs followed an interesting pattern where both copies of the PEDF gene must be present to prevent HSCs from producing massive amounts of stroma, and this is worthy of further inspection. The increased vascular density and type III collagen production may simply be a result of metastatic progression and thus only indirectly related to loss of host PEDF. PEDF+/+ contain mostly micrometastases and low-end intermediate metastases, thus we are unable to accurately compare vascular density and type III collagen production in large metastases across the three genotypes.

We envision a two-step mechanism for the progression of UM metastasis involving first the activation of HSCs and production of stroma as a scaffold for blood vessel and tumor growth, followed by the induction of angiogenesis to feed the metastasis with nutrients and oxygen. Our data suggest that host PEDF inhibits metastatic progression via both of these mechanisms. Further investigation needs to be done regarding the role of fatty liver in the progression of metastasis, as PEDF-null mice have increased liver steatosis, and this may be another mechanism regulating metastasis size.

In conclusion, host-produced PEDF clearly has a distinct role in preventing the progression of liver metastases in a mouse model of UM. This is an excellent model to study UM, as the

mice develop micrometastases, intermediate metastases, and macrometastases similar to human patients with metastatic disease. These findings suggest that host-produced PEDF may be a therapeutic target for patients with metastatic UM.

Supplementary Material

Refer to Web version on PubMed Central for supplementary material.

Acknowledgments

References

1. Singh A, et al. Uveal melanoma: trends in incidence, treatment, and survival. Ophthalmology. 2011; 118:1881–5. [PubMed: 21704381]

2. Damato B, et al. Uveal Melanoma -- Where are We Going? US Ophthalmic Review. 2011; 4(1): 105–107.

3. Hurst E, et al. Ocular melanoma: a review and the relationship to cutaneous melanoma. Archives of Dermatology. 2003; 139:1067–1073. [PubMed: 12925397]

4. Swerdlow A, et al. Risks of second primary malignancy in patients with cutaneous and ocular melanoma in Denmark, 1943–1989. International Journal of Cancer. 1995; 61:773–779.

5. Vajdic C, et al. Sun exposure predicts risk of ocular melanoma in Australia. International Journal of Cancer. 2002; 101:175–182.

6. Singh A, et al. Uveal melanoma: genetic aspects. Ophthalmology Clinics of North America. 2005; 18:85–97. [PubMed: 15763194]

7. Sato T, et al. The biology and management of uveal melanoma. Current oncology reports. 2008; 10:431–438. [PubMed: 18706273]

8. Blanco PL, et al. Uveal melanoma dormancy: an acceptable clinical endpoint? Melanoma Research. 2012; 22(5):334–340. [PubMed: 22895346]

9. Grossniklaus H, et al. Progression of Ocular Melanoma Metastasis to the Liver: the 2012 Zimmerman Lecture. JAMA Ophthalmol. 2013; 131(4):462–469. [PubMed: 23392528]

10. Lake S, et al. Comparison of Formalin-Fixed and Snap Frozen Samples Analyzed by Multiplex Ligation-Dependent Probe Amplification for Prognostic Testing in Uveal Melanoma. Anatomy and Pathology. 2012; 53(6):2647–2652.

11. Onken M, et al. Gene expression profiling in uveal melanoma reveals two molecular classes and predicts metastatic death. Cancer Res. 2004; 64(20):7205–7209. [PubMed: 15492234]

12. Vaarwater J, et al. Multiplex ligation-dependent probe amplification equals fluorescence in-situ hybridization for the identification of patients at risk for metastatic disease in uveal melanoma. Melanoma Research. 2012; 22(1):30–37. [PubMed: 22157614]

13. Vidal-Vanaclocha F, et al. The prometastatic microenvironment of the liver. Cancer Microenvironment. 2008; 1(1):113–129. [PubMed: 19308690]

14. Bakalian S, et al. Molecular pathways mediating liver metastasis in patients with uveal melanoma. Clin Cancer Res. 2008; 14(4):951–956. [PubMed: 18281525]

15. Luzzi K, et al. Multistep nature of metastatic inefficiency: dormancy of solitary cells after successful extravasation and limited survival of early micrometastases. Am J Pathol. 1998; 153(3): 865–873. [PubMed: 9736035]

16. Damato B, et al. Cytogenetics of uveal melanoma: a 7-year clinical experience. Ophthalmology. 2007; 114:1925–1931. [PubMed: 17719643]

17. Materin M, et al. Molecular Alterations in Uveal Melanoma. Curr Probl Cancer. 2011; 35(4):211–224. [PubMed: 21911184]

18. Harbour J, et al. Frequent Mutation of BAP1 in Metastasizing Uveal Melanomas. Science. 2010; 330:1410–1413. [PubMed: 21051595]

19. Marshall J, et al. Transcriptional profiling of human uveal melanoma from cell lines to intraocular tumors to metastasis. Clinical and Experimental Metastasis. 2007; 24:353–362. [PubMed: 17487557]

20. Jager M, et al. HLA expression in uveal melanoma: there is no rule without some exception. Human immunology. 2002; 63:444–451. [PubMed: 12039519]

21. Bingle L, et al. The role of tumour - associated macrophages in tumour progression: implications for new anticancer therapies. The Journal of pathology. 2002; 196:254–265. [PubMed: 11857487]

22. Beacham D, et al. Stromagenesis: the changing face of fibroblastic microenvironments during tumor progression. Seminars in Cancer Biology. 2005; 15(5):329–341. [PubMed: 15970443]

23. Zong L. 18a-Glycyrrhetinic Acid Down-Regulates Expression of Type I and III Collagen via TGF-B1/Smad Signaling Pathway in Human and Rat Hepatic Stellate Cells. International Journal of Medical Sciences. 2012; 9(5):370–379. [PubMed: 22811611]

24. Dawson D, et al. Pigment epithelium-derived factor: a potent inhibitor of angiogenesis. Science. 1999; 285:245–248. [PubMed: 10398599]

25. Fernández-Barral A, et al. Hypoxia Negatively Regulates Antimetastatic PEDF in Melanoma Cells by a Hypoxia Inducible Factor-Independent, Autophagy Dependent Mechanism. PloS one. 2012; 7(3)

26. Ho T, et al. Pigment epithelium-derived factor is an intrinsic antifibrosis factor targeting hepatic stellate cells. Am J Pathol. 2010; 177(4):1798–1811.10.2353/ajpath.2010.091085 [PubMed: 20709803]

27. Orgaz J, et al. Loss of pigment epithelium-derived factor enables migration, invasion and metastatic spread of human melanoma. Oncogene. 2009; 28(47):4147–4161. [PubMed: 19767774]

28. Bernard A, et al. Laminin receptor involvement in the anti-angiogenic activity of pigment epithelium-derived factor. Journal of Biological Chemistry. 2009; 284(16):10480–10490. [PubMed: 19224861]

29. Notari L, et al. Pigment epithelium - derived factor binds to cell - surface F1-ATP synthase. FEBS Journal. 2010; 277:2192–2205. [PubMed: 20412062]

30. Notari L, et al. Identification of a lipase-linked cell membrane receptor for pigment epithelium-derived factor. J Biol Chem. 2006; 281(49):38022–38037. [PubMed: 17032652]

31. Chen L, et al. PEDF induces apoptosis in human endothelial cells by activating p38 MAP kinase dependent cleavage of multiple caspases. Biochem Biophys Res Commun. 2006; 348(4):1288–1295. [PubMed: 16919597]

32. Volpert O, et al. Inducer-stimulated Fas targets activated endothelium for destruction by anti-angiogenic thrombospondin-1 and pigment epithelium-derived factor. Nature medicine. 2002; 8(4):349–357.

33. Cai J, et al. Pigment epithelium-derived factor inhibits angiogenesis via regulated intracellular proteolysis of vascular endothelial growth factor receptor 1. J Biol Chem. 2006; 281(6):3604–3613. [PubMed: 16339148]

34. Zhang S, et al. Pigment epithelium-derived factor downregulates vascular endothelial growth factor (VEGF) expression and inhibits VEGF-VEGF receptor 2 binding in diabetic retinopathy. J Mol Endocrinol. 2006; 37(1):1–12. [PubMed: 16901919]

35. Grippo P, Fitchev P, Bentrem D, Melstrom L, et al. Concurrent PEDF deficiency and Kras mutation induce invasive pancreatic cancer and adipose-rich stroma in mice. Gut. 2012

36. Allavena P, et al. The Yin - Yang of tumor - associated macrophages in neoplastic progression and immune surveillance. Immunological Reviews. 2008; 222:155–161. [PubMed: 18364000]

37. Notari L, et al. Pigment epithelium-derived factor is a substrate for matrix metalloproteinase type 2 and type 9: implications for downregulation in hypoxia. Invest Ophthalmol Vis Sci. 2005; 46(8):2736–2747. [PubMed: 16043845]

38. Hanahan D, et al. Patterns and emerging mechanisms of the angiogenic switch during tumorigenesis. Cell. 1996; 86(3):353–364. [PubMed: 8756718]

39. Yang H, et al. Angiostatin decreases cell migration and vascular endothelium growth factor (VEGF) to pigment epithelium–derived factor (PEDF) RNA ratio in vitro and in a murine ocular melanoma model. Mol Vis. 2006; 12:511–517. [PubMed: 16735992]

40. Yang H, et al. Constitutive overexpression of pigment epithelium-derived factor inhibition of ocular melanoma growth and metastasis. Invest Ophthalmol Vis Sci. 2010; 51(1):28–34. [PubMed: 19661223]

41. Garcia M, et al. Inhibition of xenografted human melanoma growth and prevention of metastasis development by dual antiangiogenic/antitumor activities of pigment epithelium-derived factor. Cancer Res. 2004; 64

42. Diaz C, et al. B16LS9 melanoma cells spread to the liver from the murine ocular posterior compartment (PC). Curr Eye Res. 1999; 18(2):125–129. [PubMed: 10223656]

43. Dithmar S, et al. A new technique for implantation of tissue culture melanoma cells in a murine model of metastatic ocular melanoma. Melanoma Research. 2000; 10(1):2–8. [PubMed: 10711634]

44. Cornwell M, et al. Pigment epithelium–derived factor regulates the vasculature and mass of the prostate and pancreas. Nature medicine. 2003; 9(6):774–780.

45. Chung C, et al. Anti-angiogenic pigment epithelium-derived factor regulates hepatocyte triglyceride content through adipose triglyceride lipase (ATGL). Journal of Hepatology. 2008; 48:471–478. [PubMed: 18191271]

46. Yang H, et al. In-vivo xenograft murine human uveal melanoma model develops hepatic micrometastases. Melanoma Research. 2008; 18(2):95–103. [PubMed: 18337645]

47. Yang H, et al. Low dose adjuvant angiostatin decreases hepatic micrometastasis in murine ocular melanoma model. Mol Vis. 2004; 10:987–995. [PubMed: 15623988]

48. Foss A, et al. Microvessel count predicts survival in uveal melanoma. Cancer Res. 1996; 56:2900–2903. [PubMed: 8674036]

49. Paget S. The distribution of secondary growths in cancer of the breast. The Lancet. 1889; 133(3421)

50. Folkman J. Role of angiogenesis in tumor growth and metastasis. Seminars in Oncology. 2002; 29(6):15–18. [PubMed: 12516034]

51. Gao W, et al. Serum vascular endothelial growth factor (VEGF) levels correlate with number and location of micrometastases in a murine model of uveal melanoma. British Journal of Ophthalmology. 2011; 95:112–117. [PubMed: 20819828]

52. Quintero M, et al. Hypoxia-inducible factor (HIF-1) in cancer. Eur J Surg Oncol. 2004; 5:465–468. [PubMed: 15135470]

ABBREVIATIONS

|	
H&E	Hematoxylin & eosin stain
HSCs	Hepatic stellate cells
MMP	Matrix metalloproteinases
MVD	Mean vascular density
PEDF	Pigment epithelium-derived factor
SMA	Smooth muscle actin
UM	Uveal melanoma
VEGF	Vascular endothelial growth factor
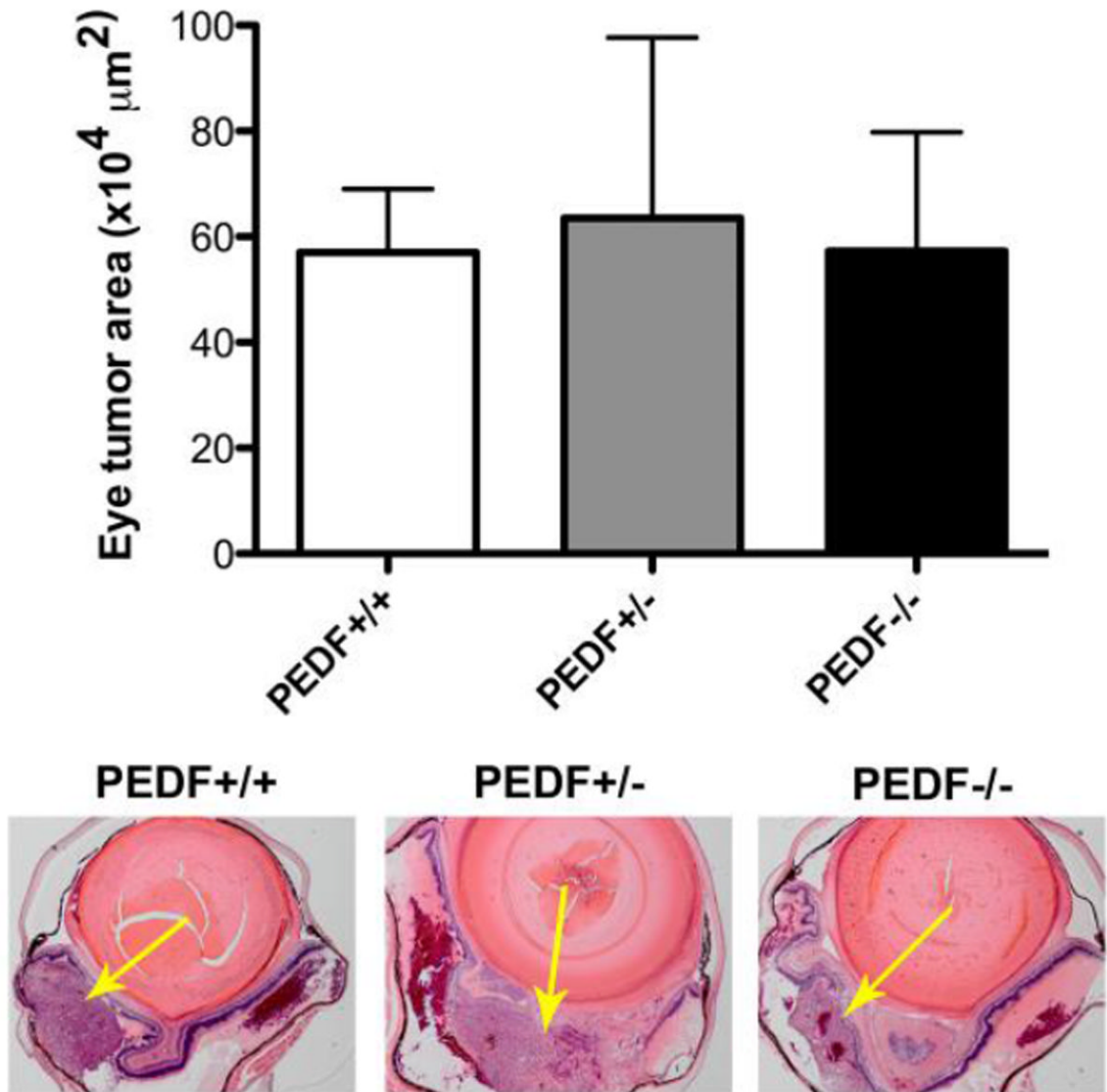
Fig. 1. Eye tumor size is not a function of mouse PEDF genotype
PEDF+/+, PEDF+/-, and PEDF-/- mice were injected with B16-LS9 cells into the posterior compartment of the right eye. One week after injection, the right eye was enucleated, sectioned, and stained by H&E. Three sections were averaged per mouse and reported as total eye tumor area. H&E images of eye tumor from PEDF+/+, PEDF+/-, and PEDF-/- mice show the equivalence in primary tumor size across genotypes. A yellow arrow highlights the primary tumor located in the posterior compartment of the eye. No statistical difference was found between each genotype of mouse. Eye and liver sections were obtained from the same set of mice. Data are reported with standard error of the mean, n=4, *p<0.05 using one-way ANOVA with Newman-Keuls post-test
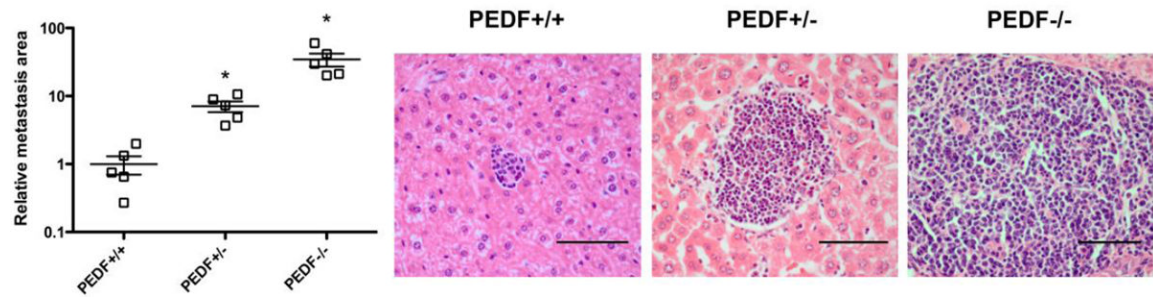
Fig. 2. Host PEDF inhibits total area of liver metastasis in a model of uveal melanoma
PEDF+/+, PEDF+/-, and PEDF-/- mice were injected with B16-LS9 cells into the posterior compartment of the right eye and allowed to metastasize over one month. Total area of metastasis coverage was measured and normalized to the total area of the liver and reported as a relative value with wild-type set to 1. Values were displayed on a scatter plot with a $\log_{10}$ scale where each box represents the averaged values of one mouse, the long bar represents the mean, and the smaller bars represent standard error of the mean, n=5, *p<0.05 using one-way ANOVA with Newman-Keuls post-test. PEDF+/- mice experienced a 7.1 fold increase in the area of liver metastasis over wild-type, and PEDF-/- mice experienced a 34.6 fold increase. Representative H&E images show metastases from PEDF+/+, PEDF+/-, and PEDF-/- mice. Eye and liver sections were obtained from the same set of mice. Black bar = 50μm
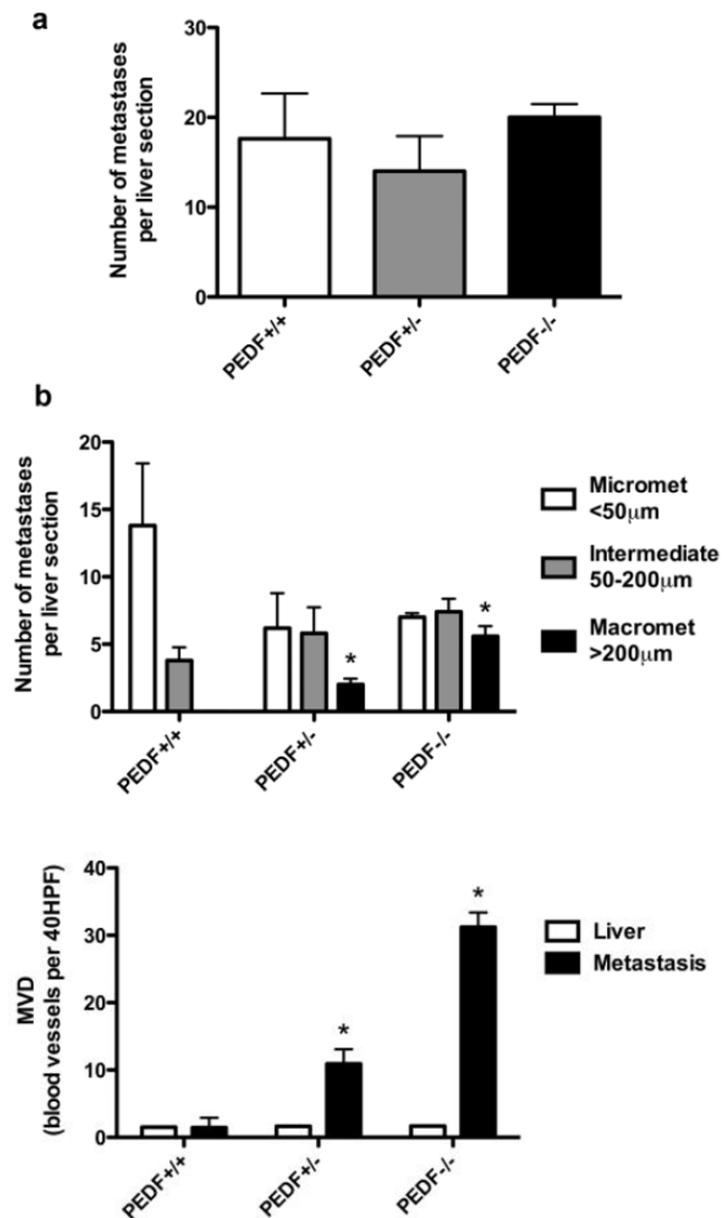
Fig. 3. The number of metastases is not a function of mouse PEDF genotype, but the number of macrometastases (diameter >200μm) increases in the absence of PEDF
a) Total count of metastases per liver section was tallied without respect to the size of each metastasis. No statistical difference was found across mouse PEDF genotypes. Data are reported with standard error of the mean, n=5, *p<0.05 using one-way ANOVA with Newman-Keuls post-test. b) The size of each individual liver metastasis from PEDF+/+, PEDF+/-, and PEDF-/- mice was measured and categorized as a micromet (diameter <50μm), an intermediate met (diameter 50-200μm), or a macromet (diameter greater than 200μm). PEDF+/+ mouse livers contained no macrometastases, while PEDF+/- and PEDF-/- mouse livers contained a progressively greater number of macrometastases. Data are reported with standard error of the mean, n=5, *p<0.05 using two-way ANOVA with Bonferroni post-test
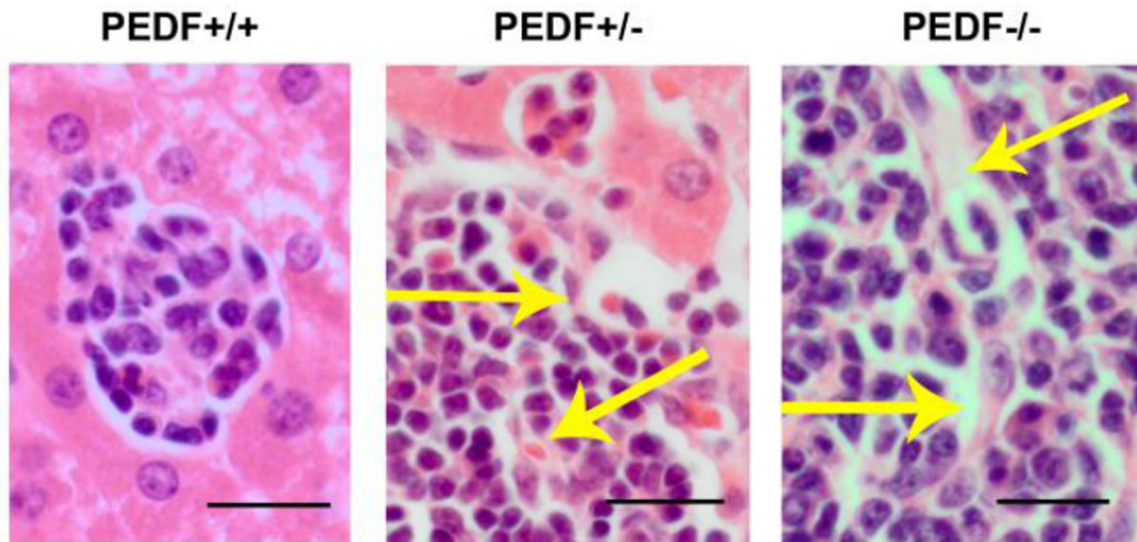
Fig. 4. Loss of PEDF is accompanied by greater vascular density within metastases
The number of blood vessels was calculated per area for each metastasis and the surrounding liver tissue and extrapolated over a full 40x high-powered field of magnification (40HPF). PEDF+/- mice had a 7.3 fold increase in the mean vascular density over wild-type mice. PEDF-/- mice showed a 20.8 fold increase in mean vascular density over wild-type mice. MVD was significantly greater in metastases than in surrounding liver tissue in both PEDF+/- and PEDF-/- mice. PEDF did not affect the MVD of surrounding liver tissue across genotypes. Metastasis and liver tissue were stained using periodic acid-Schiff without hematoxylin in order to view and count blood vessels, and shown in H&E for visual purposes. Yellow arrows point to some but not all vascular channels. Black bar = 20μm. Data are reported with standard error of the mean, n=5, *p<0.05 using one-way ANOVA with Newman-Keuls post-test
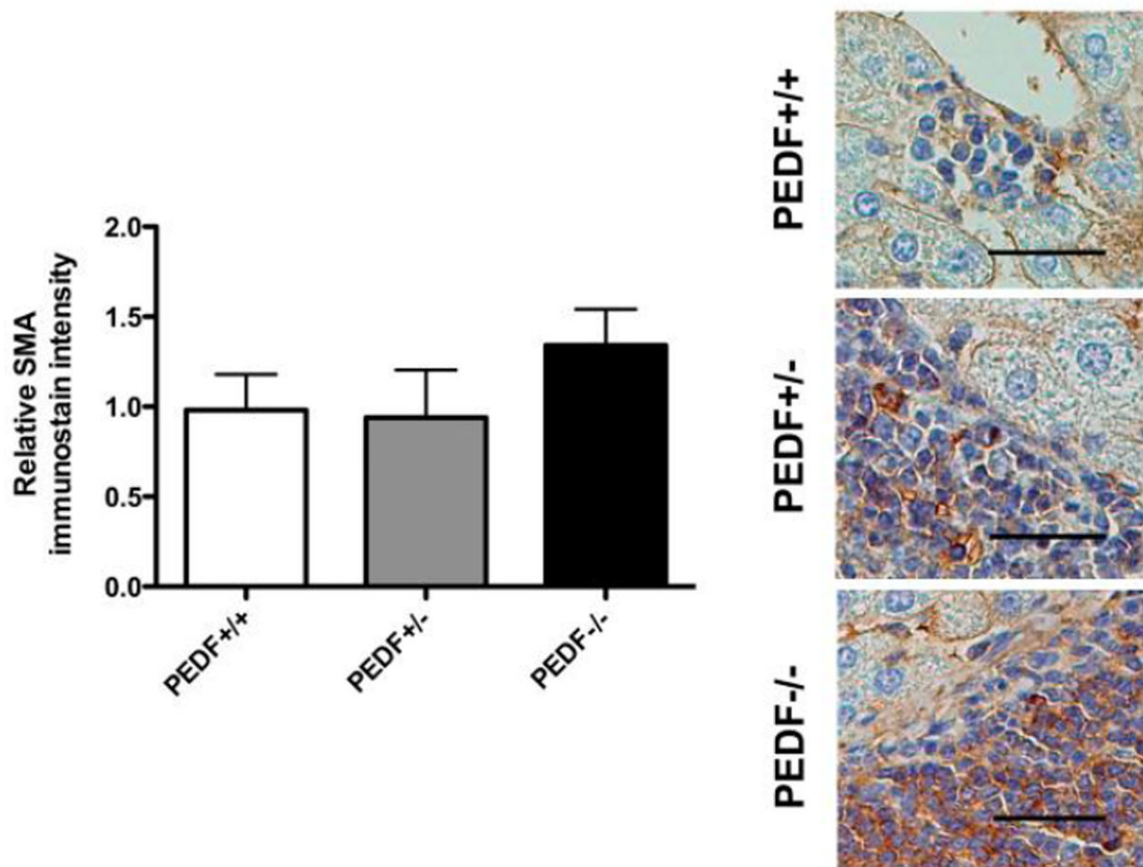
Fig. 5. Activated hepatic stellate cells were slightly more abundant in the absence of PEDF
Smooth muscle actin (SMA) immunostain intensity, a marker for activated hepatic stellate cells (HSCs), was only slightly greater in PEDF-/- metastases versus PEDF+/- and PEDF-/-, although the trend was not significant. Livers were stained with an SMA antibody to view the abundance of activated HSCs within the metastases, and no statistical difference was seen across genotypes. Representative images show SMA immunostaining (brown) in PEDF +/+, PEDF+/-, and PEDF-/- mice. Black bar = 25μm. Data are reported with standard error of the mean, n=5, *p<0.05 using one-way ANOVA with Newman-Keuls post-test
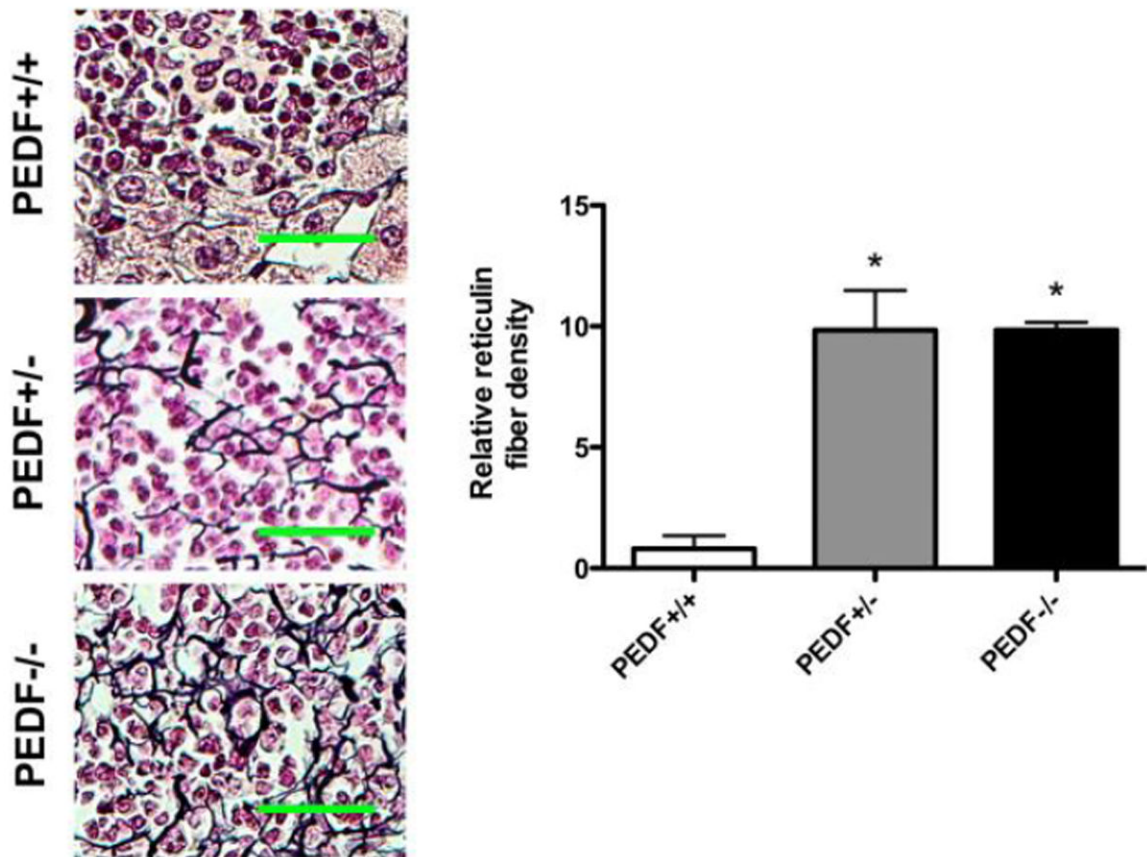
Fig. 6. Type III collagen, a stromal protein produced by hepatic stellate cells, was increased as host PEDF was lost

Reticulin stains were performed on PEDF+/+, PEDF+/-, and PEDF-/- mouse livers in order to analyze type III collagen production. Both PEDF+/- and PEDF-/- mice showed significantly greater reticulin fiber density. Representative images show reticulin fiber staining (dark purple) in PEDF+/+, PEDF+/-, and PEDF-/- mice. Fibers were traced and their lengths were summed to calculate reticulin fiber density. Green bar = 25μm. Data are reported with standard error of the mean, n=5, *p<0.05 using one-way ANOVA with Newman-Keuls post-test